Control and Simplicity in the Nanoprocessing of Semiconducting Copper-Iodine Double Chain Coordination Polymers

Javier Conesa-Egea,[†‡] Carlos. D. Redondo,[†] J. Ignacio Martínez,[#] Carlos J. Gómez-García,[ς] Óscar Castillo,[§] Félix Zamora,[†χ‡] Pilar Amo-Ochoa.[χ†*]*

[†]Departamento de Química Inorgánica, Universidad Autónoma de Madrid, 28049 Madrid, Spain.

[‡]Condensed Matter Physics Center (IFIMAC), Universidad Autónoma de Madrid, 28049 Madrid, Spain.

[#] Departamento de Nanoestructuras, Superficies, Recubrimientos y Astrofísica Molecular, Instituto de Ciencia de Materiales de Madrid (ICMM-CSIC), 28049 Madrid, Spain.

[ς]Departamento de Química Inorgánica. Instituto de Ciencia Molecular (ICMol). Parque Científico. Universidad de Valencia. Catedrático José Beltrán, 2. 46980 Paterna Valencia (Spain). Universidad de Valencia.

[§,]Departamento de Química Inorgánica, Facultad de Ciencia y Tecnología, Universidad del País Vasco, UPV/EHU, Apartado 644, 48080 Bilbao, Spain

[χ] Institute for Advanced Research in Chemical Sciences (IAdChem), Universidad Autónoma de Madrid, 28049 Madrid, Spain.

Keywords: coordination polymers, nanomaterials, multifunctional, electrical conductivity.

ABSTRACT

Two coordination polymers based on Cu(I)-I double *zig-zag* chains bearing isonicotinic acid or 3-chloroisonicotinic acid as terminal ligands, with molecular recognition capabilities, have been

synthetized and fully characterized. Both compounds present extended networks with supramolecular interactions directed by the formation of H-bonds between the complementary carboxylic groups, giving supramolecular sheets. The chloro substituent allows stablishing additional Cl···Cl supramolecular interactions that reinforce the stability of the supramolecular sheets. These coordination polymers are semiconductor materials, however the presence of chlorine produces slight changes in the I-Cu-I chains, generating a worse overlap in the Cu-I orbitals, and thus determining a decrease in its electrical conductivity value. These experimental results have also been corroborated by theoretical calculations using the study of the morphology of the density of states and 3D orbital isodensities, which determine that conductivity is mostly produced through the Cu-I skeleton and is less efficient in case of chloro derivative compound. A fast and efficient bottom-up approach based on the self-assembly of the initial building blocks and the low solutibility of these coordination polymers has been proved very useful for the production of nanostructures.

Introduction

Coordination polymers (CPs) are a large group of compounds which, depending on the selected building blocks (metal ions and organic ligands), have a great structural variety and an immense diversity of physical and chemical properties.[1] Thanks to their infinite structure and function tailorability that originates from the abundant building blocks, these materials can present, among other properties, interesting electrical conductivity.[2] For instance, the paradigmatic case of MMX chains with platinum, iodine and dithiocarboxylato ligands is particularly outstanding due to its high electrical conductivity even at room temperature, as well

as the metallic to semiconducting phase transitions showed by them with the temperature.[2e, 3] Their intriguing features have also been analyzed at the nanoscale to demonstrate their potential as a source of novel molecular wires.[2f, 4] Indeed, several CPs show significant electrical conductivity. In this context, copper(I) halides have been subjected of a number of studies, particularly for those with ligands with π* or σ* orbitals suitable for an efficient d_π metal orbitals overlapping.[1d-f, 1h, 5] As a result of their structural diversity, originating from the polymerization of copper-halogen-based subunits,[6] double Cu-X chains are a sub-class of CPs that can generate multifunctional materials showing combination of electrical conductivity and photoluminescence.[1h, 7] Moreover, the electrical conductivity found in some of the Cu-X double chains has suggested their potential use as electronic materials.[8] The features reported on copper(I) double chains with iodide as bridging ligands are also noticeable, since they show interesting luminescent properties.[1c, 1h, 6i, 7b, 9] More recently, we have found that, although this family of compounds shows rather similar structures, the double Cu-I chain presents a high degree of structural flexibility suggesting an elastic spring like behavior, when they are exposed to external physical and/or chemical stimuli.[7c] For this reason, small differences in angles and distances along the Cu-I double chains as a result of external stimuli, or even different inter-chain interactions due to the organic ligand present in the structure, modulate their electrical and optical properties.[1h, 7c] Thus, the use of organic ligands with molecular recognition capability adds to these CPs possible applications in biological or pharmacological fields.[10] However, the study of these chains using molecularly recognizable ligands is still quite limited.[7b]

In principle, the use of bottom-up methodologies seems to be suitable for the production of CP-nanostructures, due to the fact that the organic ligand-to-metal molecular recognition capability,[11] and the typically high insolubility of these materials. This is interesting, in order to

prepare nanodevices useful in disciplines such as pharmacology[12] or electronics,[13-14] depending on their properties. Nevertheless, despite their interest, the design and study of the properties of CPs at the nanoscale are still in their infancy.

For these reasons, in this work we present the synthesis in bulk and at the nanoscale of two CPs based on a double Cu-I chain with isonicotinic acid (HIN) or its derivative 3-chloroisonicotinic acid (Cl-HIN) as terminal ligands, as well as a comparative study of their structure and electrical properties, assisted by theoretical calculations.

Experimental section

Materials and methods: All reagents and solvents purchased were used without further purification. $[Cu(HIN)I]_n$ (**1**) (HIN = isonicotinic acid) was prepared following the procedures already reported.[1h] IR spectra were recorded with a PerkinElmer 100 spectrophotometer using a universal ATR sampling accessory from 4000–650 cm^{-1}. Elemental analyses were performed with a LECO CHNS-932 Elemental Analyzer. Powder X-ray diffraction data was collected using a Diffractometer PANalyticalX'Pert PRO θ/2θ primary monochromator and detector with fast X'Celerator. The samples have been analysed with scanning θ/2θ.

Preliminary direct current (*dc*) electrical conductivity measurements were performed on different single crystals of compounds $[Cu(HIN)I]_n$ (**1m**), (HIN = isonicotinic acid)[1h] and $[Cu(Cl\text{-}HIN)I]_n$ (**2m**) (Cl-HIN = 3-chloroisonicotinic acid) with graphite paste at 300 K and two contacts. The contacts were made from tungsten wires (25 mm diameter). The samples were measured at 300 K by applying an electrical current with voltages from +10 to -10 V. The measurements were performed in the compounds along the crystallographic *a* axis.

The thermal dependence of the *dc* electrical conductivity was measured with the four (or two, depending on the size of the crystal) contacts method on up to three single crystals of each

compound in the temperature range 2-400 K. The contacts were made with Pt wires (25 mm diameter) using graphite paste. The samples were measured in a Quantum Design PPMS-9 equipment connected to an external voltage source (Keithley model 2450 source-meter) and amperometer (Keithley model 6514 electrometer). All the quoted conductivity values were measured in the voltage range where the crystals are Ohmic conductors. The cooling and warming rates were 1 K min^{-1}.

Luminescence excitation and emission spectra of the solid compounds were performed at 298 K on a 48000s (T-Optics) spectrofluorometer from SLM-Aminco. A front-face sample holder was used for data collection and oriented at 608 nm to minimize light scattering from the excitation beam on the cooled R-928 photomultiplier tube. Appropriate filters were used to eliminate Rayleigh and Raman scatters from the emission. Excitation and emission spectra were corrected for the wavelength dependence of the 450 W xenon arc excitation but not for the wavelength dependence of the detection system. Spectroscopic properties were measured by reflection (front-face mode) on finely ground samples placed in quartz cells of 1 mm path length. No attempt was made to remove adsorbed or dissolved molecular oxygen from the materials. Reference samples that do not contain any fluorescent dopant were used to check the background and optical properties of the samples (see supplementary information).

The X-ray diffraction data collections and structure determinations were done with a Bruker Kappa Apex II diffractometer with graphite-monochromated $Mo_{K\alpha}$ radiation (λ = 0.71073 Å). The cell parameters were determined and refined by a least-squares fit of all reflections. A semi-empirical absorption correction (SADABS) was applied. All the structures were solved by direct methods using the SIR92 program[13] and refined by full-matrix least-squares on F^2 including all reflections (SHELXL97).[14] All non-hydrogen atoms were refined anisotropically. The hydrogen

atoms were included in their calculated positions and refined riding on the respective parent atoms. All calculations were performed using the WINGX crystallographic software package.[15] CCDC 1580668 contains the supplementary crystallographic data for this paper. These data are provided free of charge by The Cambridge Crystallographic Data Centre.

Scanning Electron Microscopy (SEM) images were taken in a Philips XL 30 S-FEG electron microscope, applying an electron beam of 300 μA intensity and 10.0 kV potential, at a pressure of 10^{-7} Pa. In order to obtain reproducible results, very flat substrates were used with precisely controlled chemical functionalities, freshly prepared just before the chemical deposition of the samples. Doped SiO_2 surfaces were sonicated for 15 min in acetone and 15 min in 2-propanol and then dried under an Argon flow. After sample preparation, the surfaces were metallized with a 10 nm thick Cr layer, at a pressure of 10^{-3} Pa.

Atomic Force Microscopy (AFM) images were registered in a Nanotec Electronica microscope, at room temperature and in an open atmosphere, using Olympus cantilevers with a constant nominal force of 0.75 N/m. Images were processed by the use of the WSxM program.[16] Doped SiO_2 surfaces were sonicated for 15 min in acetone and 15 min in 2-propanol and then dried under an Argon flow in order to obtain reproducible results.

The one-electron wave-functions are expanded in a basis of plane-waves with energy cut-offs of 400 and 500 eV for the kinetic energy and for the electronic density, respectively, which have been adjusted to achieve sufficient accuracy to guarantee a full convergence in energy and density.

Density functional theory (DFT)-based calculations were performed by using the efficient plane-wave code QUANTUM ESPRESSO.[17] In this atomistic simulation package the

Kohn−Sham equations are solved using a periodic supercell geometry. The ion−electron interaction is modeled by ultrasoft pseudopotentials,[18] and exchange-correlation (XC) effects are treated by the generalized gradient- approximation (GGA) of Perdew, Burke, and Ernzerhof (PBE).[19] The one-electron wave functions are expanded in a basis of plane-waves with energy cut-offs of 400 and 500 eV for the kinetic energy and for the electronic density, respectively, which have been adjusted to achieve sufficient accuracy in the total energy.

The Brillouin zones of the different bulk systems were sampled[20] by using a k-space of $\Delta k \leq 0.01$ Å

Synthesis of $[Cu(HIN)I]_n$ micro (1m) and (1n) submicrostructures

Copper(I) iodide (200 mg, 1.05 mmol) was dissolved in 10 mL of acetonitrile. On the other hand, isonicotinic acid (130 mg, 1.05 mmol) was dispersed in 10 mL of ethanol and added to the copper iodide solution, both at 25ºC. The resulting orange-red suspension was stirred (500 rpm) for 30 minutes and filtered to remove the unreacted ligand. A 20 µL drop of the solution was deposited on a doped SiO_2 surface and left to evaporate completely; the resulting red solid, consisting of sub-microribbons and nanofibers (**1n**), was studied by SEM (Figure 6, S7a-b). The rest of the solution was left to slowly partially evaporate at room temperature, obtaining red microcrystals[1h, 7] after 72 hours (**1m**). Total yield: 98 mg (30 % based on Cu). Elemental analysis calcd (%) for $C_6H_5CuINO_2$: C 22.88, H 1.65, N 4.47; found: C 21.34, H 1.54, N 3.92; IR selected data (ATR): $\tilde{\nu}$ (cm^{-1}) = 3444 (w), 1697 (s), 1604 (m), 1556 (m), 1411 (s), 1324 (m), 1292 (s), 1209 (m), 1133 (s), 1058 (w), 917 (w), 825 (w), 759 (m), 696 (m), 676 (m).

The DRX powder diffraction spectra show that both micrometric (**1m**) and nanometric (**1n**) crystals have the same structure (Figure S1).

Synthesis of $[Cu(Cl\text{-}HIN)I]_n$ micro (2m) and nanostructures (2n)

Copper(I) iodide (200 mg, 1.05 mmol) was dissolved in 10 mL of acetonitrile; on the other hand, 3-chloroisonicotinic acid (Cl-HIN) (167 mg, 1.05 mmol) was dispersed in 5 mL of ethanol, at 50 ºC. Both solutions were mixed and stirred (1000 rpm) at 25 ºC for 3 minutes. The resulting mixture consisted of a dark yellow solution and an orange solid consisting of $[Cu(Cl\text{-}HIN)I]_n$ nanofibers (**2n**). The solid was filtered off, washed with acetonitrile (2 x 5 mL), ethanol (2 x 5 mL) and diethyl ether (2 x 3 mL), and dried *in vacuo*. The solution was left to crystallize at room temperature, obtaining red needle-like microcrystals after 48 hours (**2m**). Total yield: 254 mg (69% based on Cu): 151 mg of nanofibers (41%) and 103 mg of microcrystals (28%). Elemental analysis calcd (%) for $C_6H_4CuIClO_2N$: C 20.69, H 1.15, N 4.02; found: C 20.93, H 1.24, N 3.88; IR selected data (ATR): $\tilde{\nu}$ (cm^{-1}) = 3024 (w), 2885 (w), 2643 (w), 2524 (w), 1711 (vs), 1698 (vs), 1589 (w), 1530 (w), 1473 (m), 1391 (vs), 1275 (vs), 1264 (vs), 1217 (vs), 1140 (w), 1090 (s), 1055 (s), 876 (m), 854 (vs), 784 (m), 733 (vs), 690 (s), 666 (vs).

The DRX powder diffraction spectra show that both, micrometric (**2m**) and nanometric (**2n**) crystals have the same structure (Figure S2).

In order to study the nanostructures by SEM (Figure 7, S7c-d), the solid (61 mg) was redispersed in 1000 µL of bidistilled water and 20 µL of the suspension were deposited on a doped SiO_2 surface. The drop was left to adsorb until it dried and the surface was purged under an argon flow.

Preparation of AFM samples of $[Cu(Cl\text{-}HIN)I]_n$ (2n)

Method A: Copper(I) iodide (200 mg, 1.05 mmol) was dissolved in 10 mL of acetonitrile; on the other hand, 3-chloroisonicotinic acid (Cl-HIN) (167 mg, 1.05 mmol) was dispersed in 5 mL of ethanol, at 50 ºC. Both solutions were mixed and stirred (1000 rpm) at 25 ºC for 3 minutes. The resulting mixture consisted of a dark yellow solution and an orange solid consisting of

$[Cu(Cl\text{-}HIN)I]_n$ nanofibers (**2n**). 400 µL of this suspension were diluted with 3600 µL of acetonitrile (dilution: 10^{-1}). 15 µL of this new suspension were deposited on a doped SiO_2 surface. The drop was left to adsorb for 1 minute and the surface was purged under an Argon flow.

Method B: Copper(I) iodide (200 mg, 1.05 mmol) was dissolved in 10 mL of acetonitrile; on the other hand, 3-chloroisonicotinic acid (Cl-HIN) (167 mg, 1.05 mmol) was dispersed in 5 mL of ethanol, at 50 ºC. Both solutions were mixed and stirred (1200 rpm) at 25 ºC for 3 minutes. The resulting mixture consisted of a dark yellow solution and an orange solid consisting of $[Cu(Cl\text{-}HIN)I]_n$ nanofibers (**2n**). 40 µL of this suspension were diluted with 3960 µL of acetonitrile (dilution: 10^{-2}). 15 µL of this new suspension were deposited on a doped SiO_2 surface. The drop was left to adsorb for 1 minute and the surface was purged under an Argon flow.

Results and Discussion

Structural characterization

The direct reactions at room temperature between CuI with isonicotinic acid[1h] and 3-chloroisonicotinic acid give rise to the fromation of Cu-I chains in which the non-modified and the chloro-functionalized isonicotinic acids coordinate to the Cu(I) centers as terminal ligands via the N atom of the aromatic rings (Figure 1). Both compounds share the feature of being based on zigzag double stranded stair chains where the copper(I) centres are bridged by μ_3-iodides. The coordination environment around each metal center is established by three bridging iodides and a pyridinic nitrogen atom arranged in a tetrahedral disposition, thus the following $[Cu(HIN)I]_n$ (**1m**) and $[Cu(Cl\text{-}HIN)I]_n$ (**2m**) chemical formulae. The copper-iodide and copper-nitrogen bond lengths are similar to those of other known, similar $[CuI(L)]_n$ stairs.[1h, 21]

Table 1. Selected distances (Å) and angles (º) in compounds **1m** and **2m**.

	1m	**2m**		**1m**	**2m**
T (K)	296	296	I1-Cu1-I1^{i}	103.02(3)	103.51(2)
Cu-I1$_{rail}$	2.6323(10)	2.6568(5)	I1-Cu1-I1^{ii}	114.24(3)	115.68(2)
Cu-I1$^{i}_{rail}$	2.6313(10)	2.6351(4)	I1^{i}-Cu1-I1^{ii}	114.27(4)	116.90(2)
Δ[Cu-I1$_{rail}$]	0.0010	0.0217	Cu1-I1-Cu1^{ii}	65.74(3)	64.32(2)
Cu-I1$^{ii}_{rung}$	2.6583(10)	2.6296(5)	Cu1-I1-Cu1$^{iii/iv}$	103.01(3)	103.51(2)
Cu-N1	2.054(5)	2.059(3)	Cu1^{ii}-I1-Cu1$^{iii/iv}$	65.75(3)	63.10(2)
Cu···Cu^{ii}	2.8715(12)	2.8141(8)	dihedral angle[a]	119.3	122.3
Cu···Cu^{iii}	2.8715(12)	2.7546(8)	tilt angle[b]	89.4	88.3
Δ[Cu···Cu]	0.0000	0.0595	twist angle[c]	61.0	57.4

Symmetry codes for **1m**: i) x, y+1, z; ii) -x+1, y+1/2, -z+3/2; iii) -x+1, y-1/2, -z+3/2; iv) x, y-1, z; for **2m**: i) x+1, y, z; ii) –x, -y, -z+2; iii) –x+1, -y, -z+2; iv) x-1, y, z. [a]Dihedral angle between adjacent Cu_2I_2 squares. [b,c]Tilting and twist angles of the pyridinic ring relative to the propagation direction of the chain.

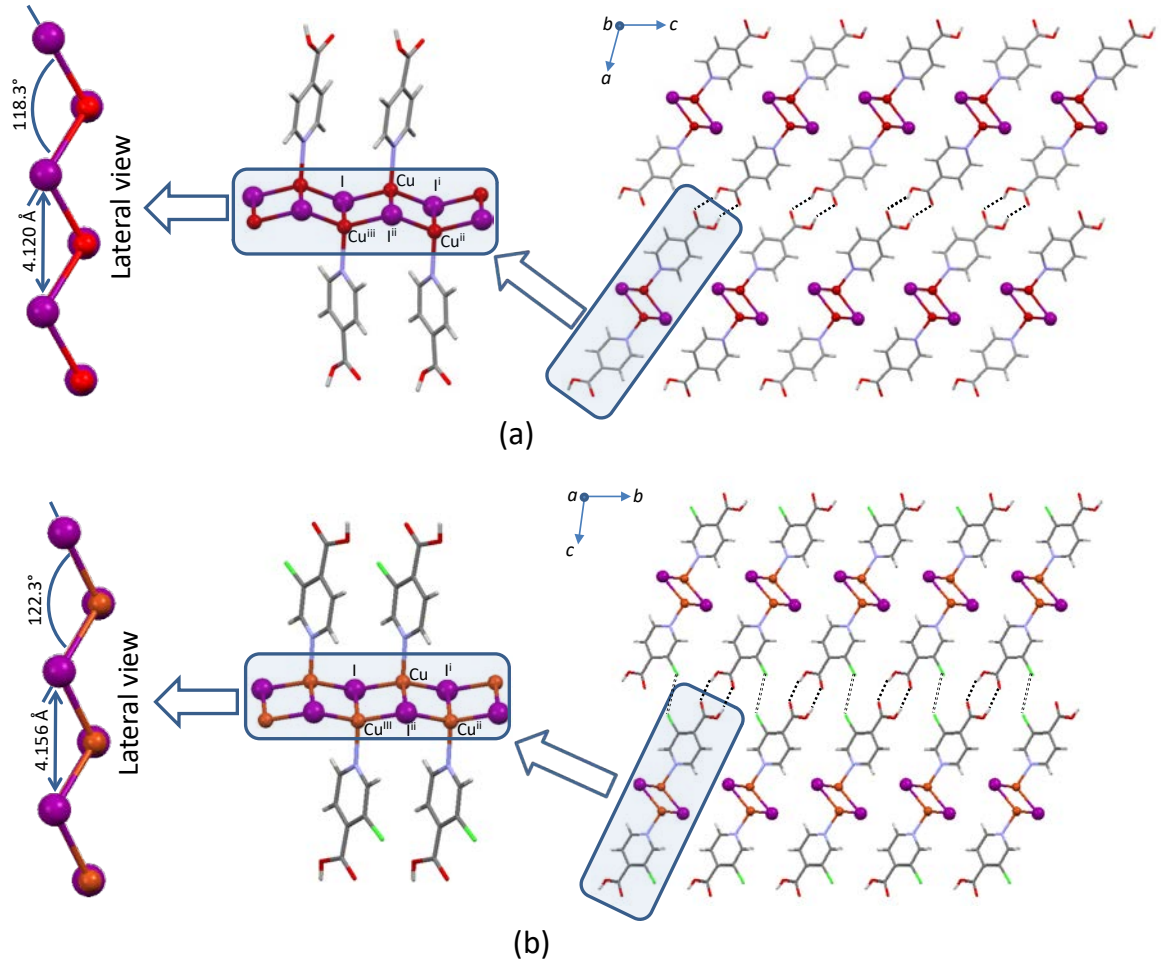

Figure 1. Crystal structure of compounds (a) $[Cu(HIN)I]_n$ (**1m**) and (b) $[Cu(Cl\text{-}HIN)I]_n$ (**2m**). Single and double dashed lines indicate hydrogen bonds and halogen···halogen interactions, respectively. Cu: orange, I: purple, Cl: green, O: red, N: blue, C: grey.

Table 1 collects the most relevant Cu-I, Cu-N and Cu···Cu bond lengths and angles for both compounds. The Cu···Cu distances within the chains found in these compounds are close to or below the sum of the Van der Waals radii (2.80 Å). The iodide is tri-coordinated in a distorted pyramidal geometry. The stair-type chain can also be described as being composed of planar Cu_2I_2 squares that share two opposite edges with angles between adjacent squares of 118.3 and 122.3º for compounds **1m** and **2m**, respectively.

The isonicotinic and 3-chloroisonicotinic acids are arranged just above and below the Cu-I core in such a way that they are oriented almost perpendicular to the propagation direction of the chain and twisted 61.0 and 57.4º, respectively. This arrangement of the terminal ligands exposes the carboxylic groups, and chloro substituent in compound **2m**, ready to establish additional supramolecular interactions. In fact, both compounds present a supramolecular structure directed by the presence of complementary hydrogen bonds between the carboxylic groups of the isonicotinic and 3-chloroisonicotinic acids belonging to adjacent chains, giving rise to planar supramolecular sheets (Figure 1). This complementary hydrogen-bonding scheme between carboxylic groups is a well-known supramolecular synthon that usually directs the supramolecular crystal structure of organic molecules containing carboxylic groups.[22] However, in the case of compound **2m** these hydrogen bonding interactions are accompanied by the presence of short Cl···Cl contacts of 3.28Å, well below the sum of the Van der Waals radii for two chlorine atoms (3.50 Å). However, the two identical C-Cl···Cl angles of 138.7º observed for this contact indicate a type I contact that usually arises from close-packing requirements and cannot be considered a major structure directing factor.[23] There are also some C-H···I contacts (H···I: 3.14 Å; C-H···I: 135.9º) among the chains that could also reinforce the stability of the supramolecular sheet. In both compounds, these sheets are only held together by means of weak Van der Waals interactions. As a consequence, the stronger interactions inside the supramolecular sheets lead to thin plate crystal morphology as found for other compounds with similar anisotropic packing forces.[24]

Characterization of physical properties

Electrical conductivity

Although electrical conductivity of copper-iodine double chain CPs is typically not very high, it is a subject of current interest because of the possibility to produce novel sensitive stimuli-response materials.[1h, 25] The room temperature conductivities values measured for **1m**[1h] and **2m** are 3×10^{-3} and 3×10^{-5} S/cm, respectively. Additionally, their electrical characterization at variable temperature confirms their semiconducting behavior, as far as the resistivity increases when the temperature decreases (see for instance scan 1 in Figure 2a). The initial activation energies are *ca*. 200 and 170 meV in **1m**[1h] and **2m**, respectively (Figure 2b). When both compounds are heated above room temperature (scan 2 in Figure 2a) they show an increase in the resistivity at ca. 380 K, suggesting the presence of a degradation process or a structural disorder.[1h] After heating at 400 K the cooling scan shows higher resistivity values in both samples, although they are still good conductors, indicating that both compounds are quite stable, in agreement with their structure, which shows the presence of strong complementary H-bonds connecting the chains (Figure 1). Interestingly, after heating the sample at 400 K, compound **2m** recovers the initial conductivity values with a smooth transition taking place at *ca*. 200 K in the cooling scan (scan 3) and ca. 260 K in the heating one (scan 4) (Figure 2a). This transition resembles the one observed in the methyl isonicotinate derivative at *ca.* 125-145 K,[1h] although in **2m** the transition is smoother. The Arrhenius plot of this cooling scan after heating the sample at 400 K in **2m** confirms the presence of the transition at ca. 200 K and shows that this sample has two semiconducting regimes after heating at 400 K. In the high temperature regime (400-220 K) compound **2m** is a semiconductor with activation energy of *ca*. 260 meV whereas, after the transition, in the low temperature regime (180-120 K), the activation energy decreases to *ca*. 100

meV (Figure 2b). Se ha resuelto la estructura a 150K, después de calentar el cristal a razón de 1ºC /min hasta 400K y luego se ha enfriado hasta 150K los datos obtenidos se han incluido en el material suplementario (tablas S2 y S3) y recogen un ligero acortamiento de las distancias metal metal y Cu-I y ligera modificación de los ángulos

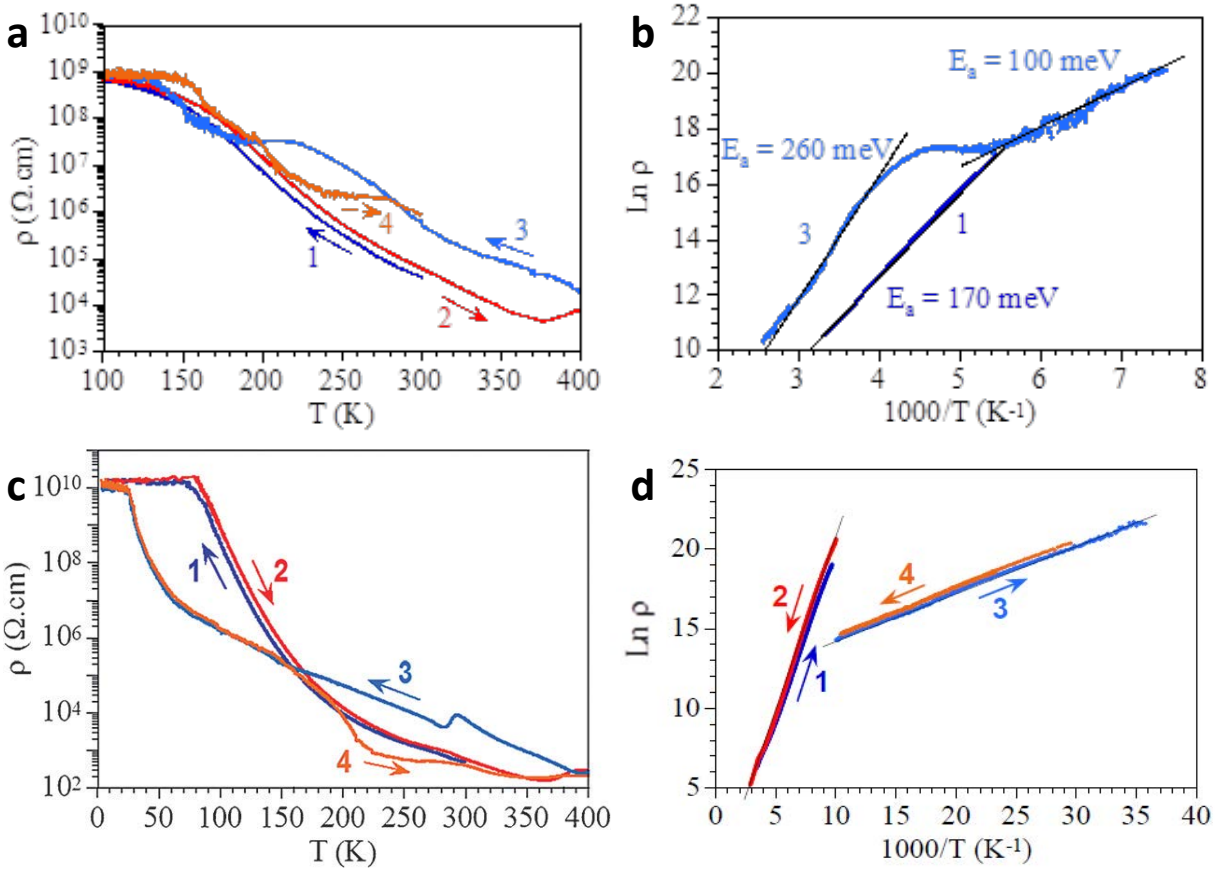

Figure 2. (a, b) Electrical behavior of compound **2m**. (a) Thermal dependence of the electrical resistivity in four successive cooling and heating scans. (b) Arrhenius plot of the first (dark blue) and second (light blue) cooling scans. (c, d) Electrical behavior of compound **1m**.[1h] (c) Thermal dependence of the electrical resistivity in four successive cooling and heating scans. (d) Arrhenius plot of the four cooling scans.

Although the similar semiconducting behavior observed in compounds **1m** and **2m** agrees with the similar structure shown by both compounds, the room temperature conductivity value is two

orders of magnitude higher in compound **1m** ($3x10^{-3}$ S/cm in **1m** *vs*. $3x10^{-5}$ S/cm in **2m**). If we look at the Cu···Cu distances along the chain in both compounds (Table 1, Figure 3) we can see that this distance is significantly shorter in **2m** (2.8141(8) Å) than in **1m** (2.8715(12) Å), suggesting that the conductivity should be much higher in **2m**. This fact indicates that the electron delocalization does not takes place through direct Cu···Cu interactions (because they are too long in all the cases), as already observed in the series of similar $[Cu(L)I]_n$ chains with isonicotinic acid (**1m**) and the methyl and ethyl isonicotinate esters.[1h] We can, therefore, conclude that, as in the mentioned similar $[Cu(L)I]_n$ chains,[1h] the conductivity must take place through the Cu-I_{rail} bonds along the chain. These bond lengths are longer for compound **2m** (average value = 2.6460(5) Å) than for **1m** (average value = 2.6318(10) Å, Table 1), in agreement with the lower conductivity observed in **2m**. A second structural parameter that may determine the electron delocalization and, thus, the conductivity, is the dimerization of these Cu-I_{rail} distances. As can be seen in Table 1, this dimerization (measured as the difference between the two alternating Cu-I_{rail} distances) is much higher in **2m** (0.0217 Å) than in **1m** (0.0010), again in agreement with the higher resistivity in **2m**. A third parameter that may influence the conductivity is the I-Cu-I bond angle along the chain. This angle is slightly larger in **2m** (103.51(2)º in **2m** vs. 103.02(3)º in **1m**, Figure 3), resulting in a worse overlap of the Cu and I orbitals in **2m** (which is maximum for a I-Cu-I angle of 90º). Again this worse overlap in **2m** agrees with the higher resistivity measured in **2m**. A fourth structural parameter that also may determine the electrical conductivity is the dihedral angle between the Cu_2I_2 square units along the chain. This dihedral angle also determines the orbital overlap with a maximum at 90º. Compound **1m** has a dihedral angle closer to 90º than **2m** (119.3º *vs*. 122.3º) and, accordingly, it must present a better orbital overlap and, thus, a lower resistivity value, in agreement with the

experimental results. In summary, the four structural parameters (Cu-I_{rail} bond lengths, dimerization along the chain, I-Cu-I bond angles and dihedral angle between the Cu_2I_2 units along the chain) point to a better conductivity for compound **1m**, in agreement with the measured values.

Finally, the recovery of the electrical resistivity at *ca*. 200-260 K observed in compound **2m** may be attributed to a possible smooth reversible structural transition implying a slight change in the dimerization of the chain, as was observed in the closely related chain with the methyl isonicotinate ester $[Cu(MeIN)I]_n$.[1h] This observation agrees with the sensitive character of the Cu-I double chain.

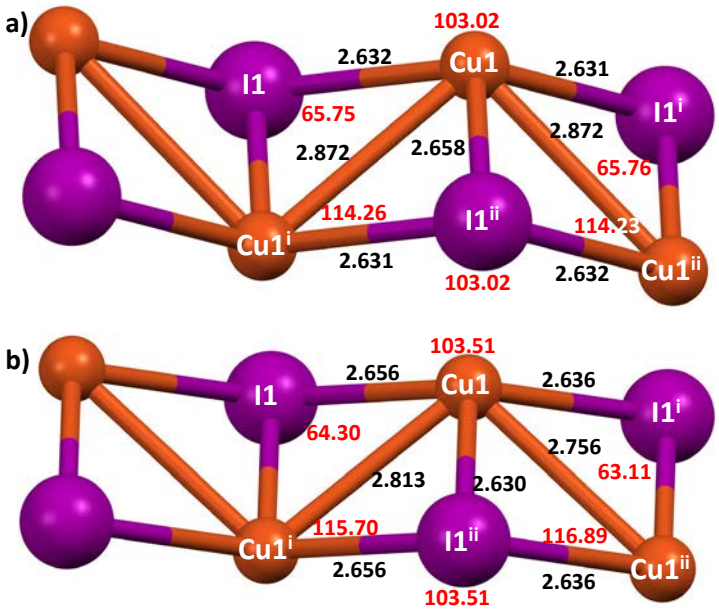

Figure 3. Cu-I bond distances (black) and angles (red) in compounds $[Cu(HIN)I]_n$ (**1m**) (a) and $[Cu(Cl\text{-}HIN)I]_n$ (**2m**) (b).

Theoretical Calculations

To rationalize from a theoretical point of view the electronic conductivity results obtained for compounds $[Cu(HIN)I]_n$ (**1m**) and $[Cu(Cl\text{-}HIN)I]_n$, (**2m**) we have carried out a battery of first-

principles density functional theory (DFT)-based calculations (see Experimental Section for computational details). In the theoretical simulations, we have used the atomic coordinates found in the X-ray structures of both compounds to evaluate the real geometry of the materials in the crystalline phase, in which the electrical measurements were carried out. For the compounds, the residual forces acting on each atom in all the calculations were below 0.1 eV/Å, which is low enough to guarantee perfectly converged and realistic results for such complex systems from a theoretical point of view. This noticeably good geometrical transferability between the experimental configurations and our theoretical implementation has already provided successful results for other similar polymer crystals.[1h]

Figure 4 shows the DFT-based computed density of electronic states (in eV^{-1}) as a function of the energy (in eV; referred to the Fermi level of each compound) for compounds $[Cu(HIN)I]_n$ (**1m**) (Figure 4a) and $[Cu(Cl\text{-}HIN)I]_n$ (**2m**) (Figure 4b). The morphology and electronic properties of compound **1m** has been previously reported and discussed,[1h] and herein we will compare them with those computed for compound **2m**. For the case of compound $[Cu(Cl\text{-}HIN)I]_n$ (**2m**), the density of states (Figure 4b) reveals a very small VB-CB gap of around 0.05 eV, to be compared with that of 0.13 eV obtained for the compound $[Cu(HIN)I]_n$. Interestingly, in compound **2m** both the valence and the conduction bands are very localized, corresponding to the two clear isolated peaks establishing such a small gap. However, although compound $[Cu(HIN)I]_n$ (**1m**) (Figure 4a) shows a slightly higher VB-CB gap of 0.13 eV, in this case the valence and conduction bands are visibly more hybridized and mixed with deeper and less bounded states, respectively. Although both gap values are slightly different, the morphology of the density of states profiles is also remarkably different at low temperature, which seems to define the electronic properties of both compounds and can help to rationalize their dissimilar

behavior regarding the different values of electrical conductivity of both polymers. The lower band gap, 0.05 eV, is obtained for compound **2m**; nevertheless, this is the compound yielding a lower conductivity value, 3×10^{-5} S cm^{-1}. On the contrary, it is for the $[Cu(HIN)I]_n$ (**1m**) compound, with a slightly higher gap of 0.13 eV, that a higher value of the electrical conductivity, 3×10^{-3} S cm^{-1}, is measured. This apparently anomalous effect it is not such, and can be easily rationalized just regarding the morphology of the density of states.

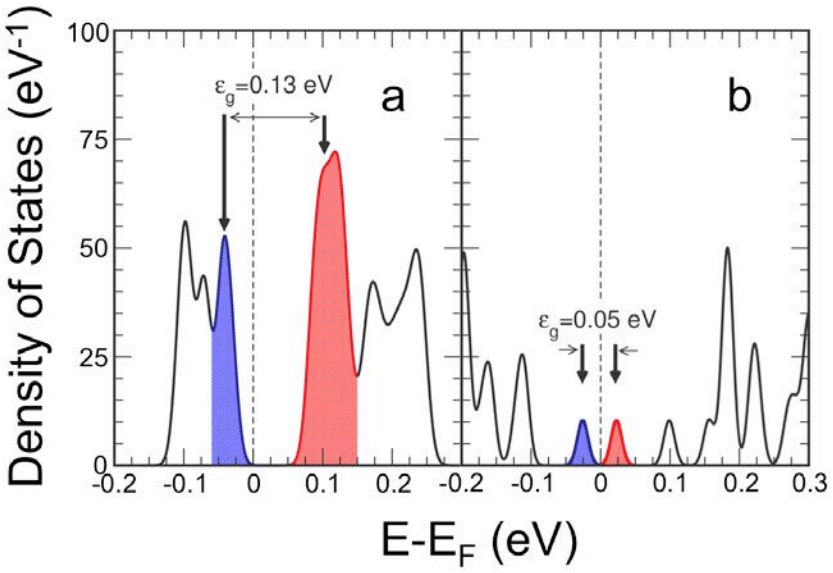

Figure 4. Computed total density of electronic states (in eV^{-1}) for $[Cu(HIN)I]_n$ (**1m**) (a) and $[Cu(Cl\text{-}HIN)I]_n$ (**2m**) (b) as a function of the energy (in eV), relative to the Fermi level. Each energy level has been broadened with a Lorentzian profile with a line width of 0.01 eV, and the valence and conduction bands for both compounds have been shaded in blue and red, respectively. Values of the VB-CB band-gaps are shown superimposed to each corresponding panel.

The fact that compound **1m** shows a valence band highly hybridized and mixed with deeper states will undoubtedly favor the supplying of electronic carriers towards the conduction band, which, at the same time, is also visibly hybridized with a bunch of less bounded states very close

in energy producing a broad overlapped CB also reinforcing the conduction. The broad and hybridized valence band in **1m** acts as a sort of electronic charge reservoir making the conduction process more efficient than for the case of the compound **2m** that, even showing a lower value of the gap, the delocalization of both VB and CB blocks the efficiency of the conduction in comparison with **1m**. The VB and CB 3D morphology is shown (Figure 5) and explained below, and reinforces the aforementioned comments. On the other hand, at this point it is important to remark that, although we can give a rationalized explanation to the previous anomalous effect, there is a quantity experimentally obtained that seems to scale with the computed band gaps: the activation energy. The initial activation energies for compounds **1m** and **2m** are 200 and 170 meV, values that agree with the band gaps theoretically obtained of 0.13 and 0.05 eV, respectively.

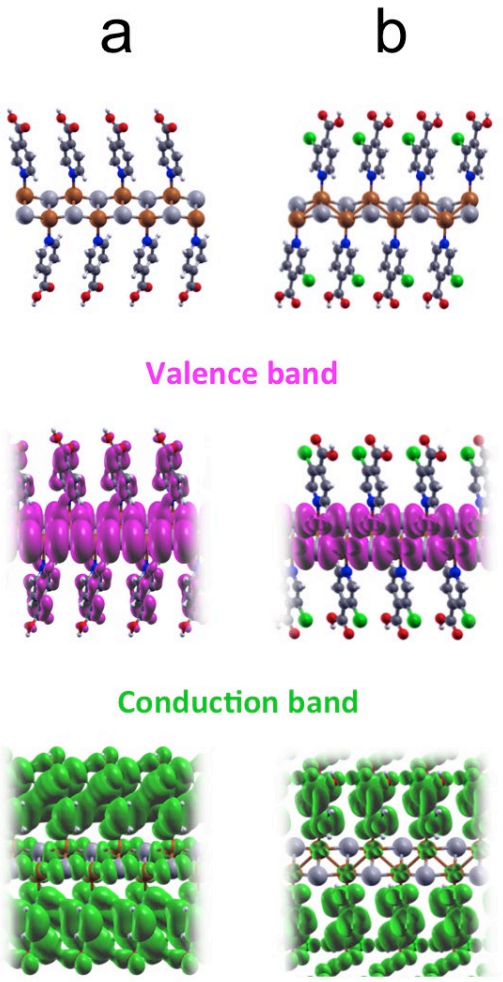

Figure 5. Computed 3D orbital isodensities corresponding to the valence (middle panels) and conduction (bottom panels) bands (all with a value of 10^{-4} e^{-} $Å^{-3}$) for the compounds $[Cu(HIN)I]_n$ (**1m**) (a) and $[Cu(Cl\text{-}HIN)I]_n$ (**2m**) (b). Clean geometries are also shown (top panels) for better visualization.

Figure 5 shows the 3D orbital isodensities corresponding to the valence and conduction bands (all with a value of 10^{-4} e-$Å^{-3}$) for compounds $[Cu(HIN)I]_n$ (**1m**) (Figure 5a) and $[Cu(Cl\text{-}HIN)I]_n$ (**2m**) (Figure 5b). In this figure it is possible to appreciate that, in **1m**, the electron valence band is mostly located along the Cu–I skeleton, whilst the conduction band shows a continuous orbital side-to-side hybridization formed between the ligands. Thus, the conduction will be produced

mainly along the one-dimensional chains. This is in agreement with the structural data, which show that the Cu-I distances for this compound **1m** are shorter than for compound **2m** favoring the conduction. Additionally, the valence band shows some significant weight also within the organic ligands, which may ease the carriers' mobility towards the conduction band, mostly located on these ligands.

On the contrary, for compound $[Cu(Cl\text{-}HIN)I]_n$ (**2m**) the valence band is totally and only located in the metal chain. However, if we observe the conduction band of this compound, it is located almost exclusively in the ligands, and the small contribution that has in the chain is only in the Cu atoms of the metal chain, where it is possible to observe orbitals with a highly atomic character and very clear morphology dz^2. In this case, the isodensities show significantly less hybridization and overlapping in the states located in the ligands of the conduction band and the states are much localized in both the VB and CB, with no mixed contribution of ligands in BV or of metallic skeleton in BC, which will hinder the conduction effectivity, in agreement with the experimental results.

Morphology studies

The methodology applied to reduce the size of the CPs is a bottom-up approaching, starting from the building blocks and taking advantage of the high insolubility of the CPs in the reaction solvent.

Micro and sub-microfibers with dimensions of (1.7 ± 0.9) x (11 ± 7) μm^2 and (0.304 ± 0.082) x (6 ± 1) μm^2, respectively for compound $[Cu(HIN)I]_n$ (**1n**) where obtained by fast evaporation at room temperature of a drop of a suspension of copper(I) iodide and isonicotinic acid on a SiO_2 surface, (Figure 6b-d). Bigger microcrystals of $[Cu(HIN)I]_n$ **(1m**) with mean dimensions of (85 ± 63) x (1244 ± 549) μm^2 have been obtained from the mother liquor by slow evaporation during

72 h (Figure 6a). The extremely high insolubility of isonicotinic acid prevents the immediate formation of **1n** nanostructures in the reaction medium.

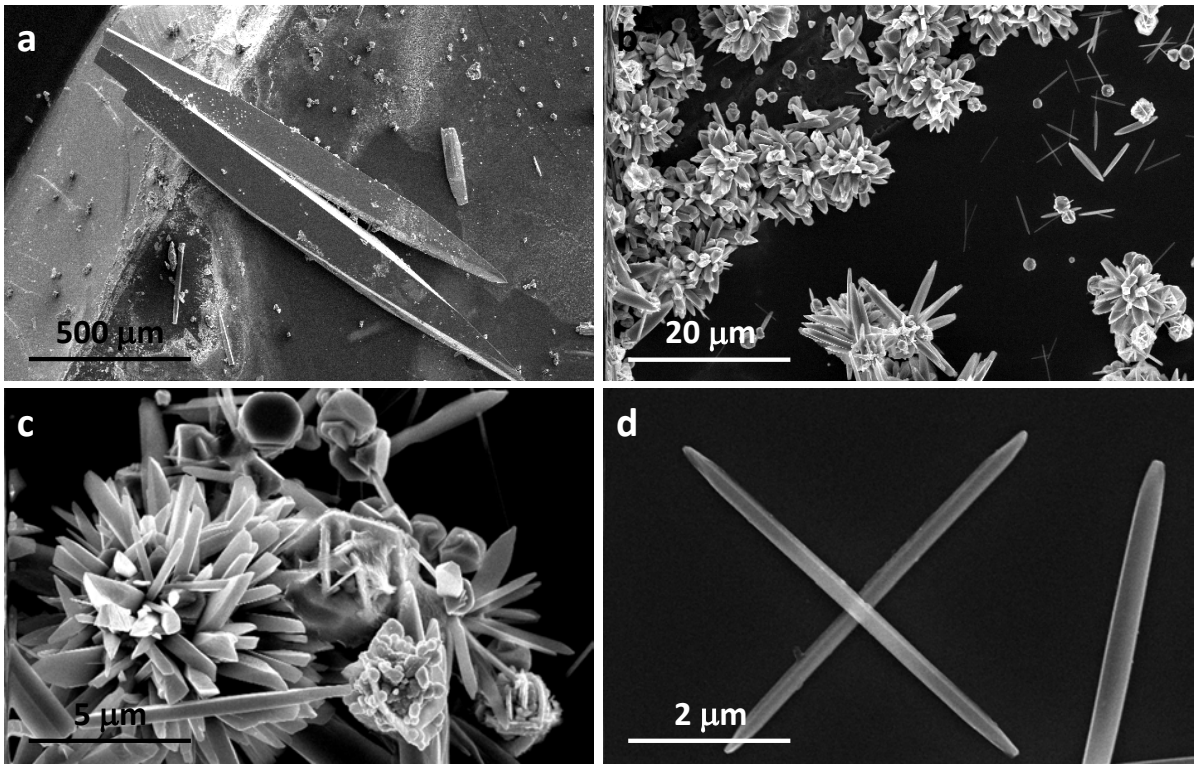

Figure 6. (a) SEM image of compound $[Cu(HIN)I]_n$ (**1n**) microcrystals obtained by slow evaporation of the mother solution. (b) General SEM image of compound $[Cu(HIN)I]_n$ (**1n**) micro and sub-microfibers obtained by fast evaporation of a 20 µL drop of the mother solution (52 mM). (c) Detailed SEM image of the razor-like microfibers of compound $[Cu(HIN)I]_n$ (**1n**). (d) Detailed SEM image of the sub-microfibers of compound $[Cu(HIN)I]_n$ (**1n**).

In a similar way, the direct reaction between copper(I) iodide and 3-chloroisonicotinic acid at room temperature leads to the immediate formation of thinner straight nanofibers of compound $[Cu(Cl\text{-}HIN)I]_n$ (**2n**) with mean dimensions of (0.08 ± 0.02) x (0.8 ± 0.3) x (40 ± 11) μm^3 (Figure 7b-d). Again, slow evaporation of the mother solution (48 h) produces microcrystals with mean dimensions of (33 ± 11) x (387 ± 40) μm^2 (Figure 7a).

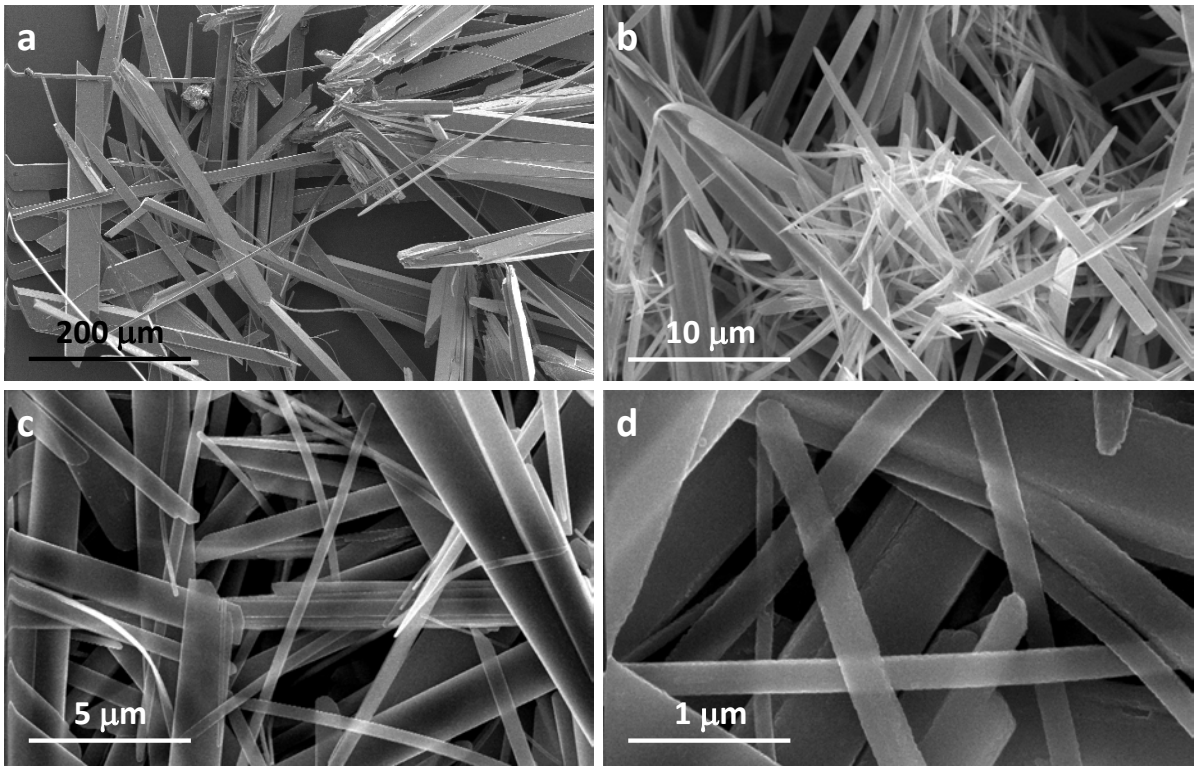

Figure 7. (a) SEM image of microcrystals of compound $[Cu(Cl\text{-}HIN)I]_n$ (**2m**) obtained by direct reaction at 25ºC between CuI and the Cl-HIN ligand in CH_3CN/EtOH, after 2 days of slow evaporation: large area (bar-scale 200 μm). (b, c, d) General and detailed SEM images of compound $[Cu(Cl\text{-}HIN)I]_n$ (**2n**) nanofibers obtained after 3 minutes of reaction time.

Direct evidence of nanofibers formation of $[Cu(Cl\text{-}HIN)I]_n$ (**2n**) has been observed by Atomic Force Microscopy (AFM). This has been done using the bottom-up methodology with strong magnetic stirring (>1000 rpm) in the synthesis medium, to minimize the inter-chain hydrogen bonding interactions between the carboxylic groups of the 3-chloroisonicotinic acid ligands present in polymer **2n**. Figure 8 shows two AFM topography images of **2n** showing fibers with heights between 5-15 nm, which are in good agreement with the height expected for a bunch of 5-14 chains of **2n**, taking into account the height found by single crystal X-ray diffraction for an individual chain (Figure 1b) whose value is about 11 Å (1.1 nm).

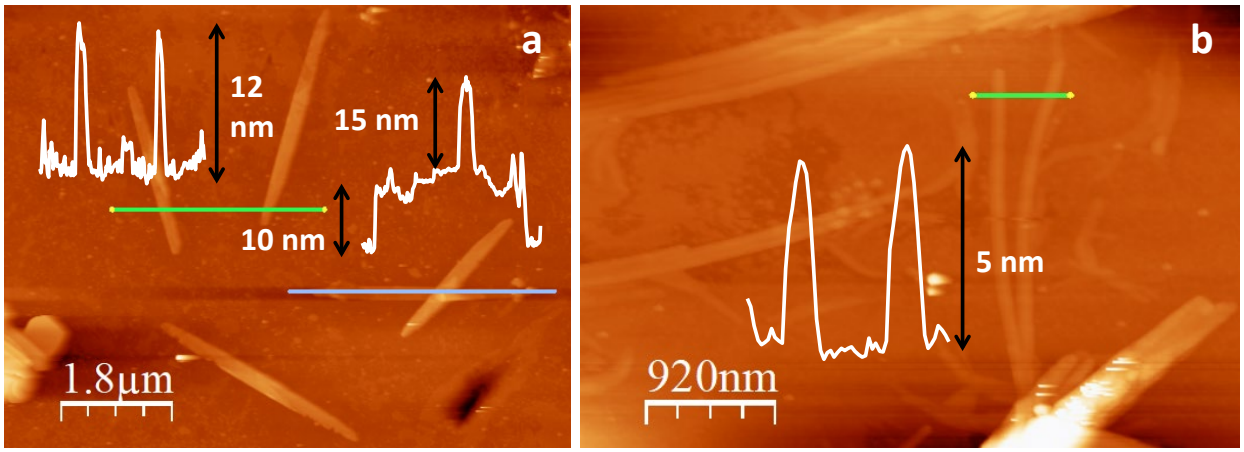

Figure 8. AFM images of nanofibers of compound $[Cu(Cl\text{-}HIN)I]_n$ (**2n**) on SiO_2 prepared by magnetic stirring (1200 rpm) and drop casting, with their height profiles across the green and blue lines.

Conclusions

Two 1D coordination polymers: $[Cu(HIN)I]_n$ and $[Cu(Cl\text{-}HIN)I]_n$, based on CuI and two similar molecular organic ligands with recognition capability (isonicotinic acid, HIN, and 3-chloroisonicotinic acid, Cl-HIN) have been synthetized. Apart from the 2D supramolecular sheets formed by the H-bonds between the carboxylic groups present in both compounds, the presence of the Cl substituent in $[Cu(Cl\text{-}HIN)I]_n$ produces an additional supramolecular Cl···Cl interaction. These polymers are semiconductors with one of the highest electrical conductivity values reported for a copper(I) halide coordination polymer.[26]

As we have published before, this kind of Cu-I zig zag chains are really interesting materials where small variations in their -I-Cu-I-Cu- distances and angles are responsible for their electrical differences even they are structurally very similar. We can show that Cu-Cu distances are not the key factor to improve the electrical conductivity, being sometimes the Cu-I distance the most plausible pathway for the electronic delocalization.

The morphology of the density of states calculated by DFT for both compounds shows a more efficient conduction process in polymer $[Cu(HIN)I]_n$, and the 3D orbital isodensities allow to appreciate that the electron valance band of this compound is located mainly along Cu-I skeleton, in agreement with the fact that the small variations in these distances are key to increase the electrical conductivity value.

A simple adjustment of reaction conditions allows that the building blocks directly form nanostructures, which are potentially useful materials for their implementation in nanoelectronics.

Supporting Information.

The supporting information is available free of charge. X-ray single crystal diffraction analysis of compound [Cu(Cl-HIN)I]n at different temperatures (CIF). X Ray powder diffraction, thermogravimetric, emission and electrical studies and SEM and AFM images of [Cu(Cl-HIN)I]n (PDF).

Acknowledgments

We thank the Spanish MINECO (projects MAT2013-46753-C2-1-P, MAT2013-46502-C2-1 and 2-P, MAT2016-75883-C2-2-P and CTQ2017-87201-P, fellowship BES-2015-071534) and the Generalitat Valenciana (PrometeoII/2014/076 project) for financial support.

Abbreviations

CP: coordination polymer, HIN: isonicotinic acid, Cl-HIN: 3-chloroisonicotinic acid, SEM: Scanning Electron Microscopy, AFM: Atomic Force Microscopy.

REFERENCES

(1) aA. El-Shekeil, H. Al-Maydama, A. Al-Karbooly, M. A. Khalid, *Polymer* **1999**, *40*, 2879-2887; bS.-J. Kim, M. Matsumoto, K. Shigehara, *Synthetic Met* **1999**, *107*, 27-33; cD. M. Ciurtin, N. G. Pschirer, M. D. Smith, U. H. F. Bunz, H.-C. zur Loye, *Chemistry of Materials* **2001**, *13*, 2743-2745; dP. Nagels, R. Mertens, H. O. Desseyn, *Synthetic Met* **2002**, *128*, 1-6; eJ. H. Yu, J. Q. Xu, L. Ye, H. Ding, W. J. Jing, T. G. Wang, J. N. Xu, H. B. Jia, Z. C. Mu, G. D. Yang, *Inorg Chem Commun* **2002**, *5*, 572-576; fC. B. Aakeroy, A. M. Beatty, J. Desper, M. Oshea, J. Valdes-Martinez, *Dalton T* **2003**, 3956-3962; gJ. P.

García-Terán, O. Castillo, A. Luque, U. García-Couceiro, P. Román, F. Lloret, *Inorg Chem* **2004**, *43*, 5761-5770; hK. Hassanein, J. Conesa-Egea, S. Delgado, O. Castillo, S. Benmansour, J. I. Martinez, G. Abellan, C. J. Gomez-Garcia, F. Zamora, P. Arno-Ochoea, *Chem-Eur J* **2015**, *21*, 17282-17292.

(2) aP. Amo-Ochoa, S. S. Alexandre, S. Hribesh, M. A. Galindo, O. Castillo, C. J. Gómez-García, A. R. Pike, J. M. Soler, A. Houlton, F. Zamora, *Inorg Chem* **2013**, *52*, 5290-5299; bP. Amo-Ochoa, O. Castillo, S. S. Alexandre, L. Welte, P. J. de Pablo, M. Isabel Rodriguez-Tapiador, J. Gomez-Herrero, F. Zamora, *Inorg Chem* **2009**, *48*, 7931-7936; cP. Amo-Ochoa, O. Castillo, C. J. Gomez-Garcia, K. Hassanein, S. Verma, J. Kumar, F. Zamora, *Inorg Chem* **2013**, *52*, 11428-11437; dR. Mas-Balleste, J. Gomez-Herrero, F. Zamora, *Chem Soc Rev* **2010**, *39*, 4220-4233; eL. Welte, A. Calzolari, R. Di Felice, F. Zamora, J. Gomez-Herrero, *Nat Nano* **2010**, *5*, 110-115; fJ. Gómez-Herrero, F. Zamora, *Adv Mater* **2011**, *23*, 5311-5317; gG. Givaja, P. Amo-Ochoa, C. J. Gomez-Garcia, F. Zamora, *Chem Soc Rev* **2012**, *41*, 115-147; hX. Zhang, W. Liu, G. Z. Wei, D. Banerjee, Z. Hu, J. Li, *Journal of the American Chemical Society* **2014**, *136*, 14230-14236.

(3) aM. Mitsumi, T. Yamashita, Y. Aiga, K. Toriumi, H. Kitagawa, T. Mitani, M. Kurmoo, *Inorg Chem* **2011**, *50*, 4368-4377; bH. Kitagawa, T. Mitani, *Coordination Chemistry Reviews* **1999**, *192*, 1169-1184; cM. Mitsumi, T. Murase, H. Kishida, T. Yoshinari, Y. Ozawa, K. Toriumi, T. Sonoyama, H. Kitagawa, T. Mitani, *Journal of the American Chemical Society* **2001**, *123*, 11179-11192.

(4) M. Mitsumi, S. Umebayashi, Y. Ozawa, K. Toriumi, H. Kitagawa, T. Mitani, *Chem Lett* **2002**, 258-259.

(5) J.-C. Li, H.-X. Li, H.-Y. Li, W.-J. Gong, J.-P. Lang, *Cryst Growth Des* **2016**, *16*, 1617-1625.

(6) aS. Perruchas, C. Tard, X. F. Le Goff, A. Fargues, A. Garcia, S. Kahlal, J.-Y. Saillard, T. Gacoin, J.-P. Boilot, *Inorg Chem* **2011**, *50*, 10682-10692; bJ. Pospisil, I. Jess, C. Nather, M. Necas, P. Taborsky, *New J Chem* **2011**, *35*, 861-864; cA. Gallego, O. Castillo, C. J. Gómez-García, F. Zamora, S. Delgado, *Inorg Chem* **2012**, *51*, 718-727; dW.-W. Zhou, W. Zhao, X. Zhao, F.-W. Wang, B. Wei, *Synthesis and Reactivity in Inorganic, Metal-Organic, and Nano-Metal Chemistry* **2013**, *43*, 1171-1174; eN. Kitada, T. Ishida, *Crystengcomm* **2014**, *16*, 8035-8040; fS. Maderlehner, M. J. Leitl, H. Yersin, A. Pfitzner, *Dalton T* **2015**, *44*, 19305-19313; gC. Slabbert, M. Rademeyer, *Coordination Chemistry Reviews* **2015**, *288*, 18-49; hY. Song, R. Q. Fan, P. Wang, X. M. Wang, S. Gao, X. Du, Y. L. Yang, T. Z. Luan, *Journal of Materials Chemistry C* **2015**, *3*, 6249-6259; iA. N. Dou, Y. C. Du, Q. L. Chen, K. L. Luo, C. Zhang, A. X. Zhu, Q. X. Li, *Z Anorg Allg Chem* **2016**, *642*, 731-735; jJ. Troyano, J. Perles, P. Amo-Ochoa, J. I. Martínez, M. Concepción Gimeno, V. Fernández-Moreira, F. Zamora, S. Delgado, *Chemistry – A European Journal* **2016**, n/a-n/a; kJ. Troyano, J. Perles, P. Amo-Ochoa, F. Zamora, S. Delgado, *Crystengcomm* **2016**.

(7) aP. Amo-Ochoa, K. Hassanein, C. J. Gómez-García, S. Benmansour, J. Perles, O. Castillo, J. I. Martínez, P. Ocón, F. Zamora, *Chem. Commun. DOI: 10.1039/C5CC04746C* **2015**; bK. Hassanein, P. Amo-Ochoa, C. J. Gomez-Garcia, S. Delgado, O. Castillo, P. Ocon, J. I. Martinez, J. Perles, F. Zamora, *Inorg Chem* **2015**, *54*, 10738-10747; cP. Amo-Ochoa, K. Hassanein, C. J. Gomez-Garcia, S. Benmansour, J. Perles, O. Castillo, J. I. Martinez, P. Ocon, F. Zamora, *Chem Commun* **2015**, *51*, 14306-14309.

(8) P. Amo-Ochoa, L. Welte, R. Gonzalez-Prieto, P. J. Sanz Miguel, C. J. Gomez-Garcia, E. Mateo-Marti, S. Delgado, J. Gomez-Herrero, F. Zamora, *Chem Commun* **2010**, *46*, 3262-3264.
(9) aN. M. Khatri, M. H. Pablico-Lansigan, W. L. Boncher, J. E. Mertzman, A. C. Labatete, L. M. Grande, D. Wunder, M. J. Prushan, W. G. Zhang, P. S. Halasyamani, J. Monteiro, A. de Bettencourt-Dias, S. L. Stoll, *Inorg Chem* **2016**, *55*, 11408-11417; bS. Demir, H. M. Cepni, N. Bilgin, M. Holynska, F. Yilmaz, *Polyhedron* **2016**, *115*, 236-241; cA. Aguirrechu-Corneron, R. Hernandez-Molina, P. Rodriguez-Hernandez, A. Munoz, U. R. Rodriguez-Mendoza, V. Lavin, R. J. Angel, J. Gonzalez-Platas, *Inorg Chem* **2016**, *55*, 7476-7484; dW. Ji, J. Qu, S. Jing, D. R. Zhu, W. Huang, *Dalton T* **2016**, *45*, 1016-1024; eE. Cariati, E. Lucenti, C. Botta, U. Giovanella, D. Marinotto, S. Righetto, *Coordination Chemistry Reviews* **2016**, *306*, 566-614.
(10) aV. G. Vegas, R. Lorca, A. Latorre, K. Hassanein, C. J. Gómez-García, O. Castillo, Á. Somoza, F. Zamora, P. Amo-Ochoa, *Angewandte Chemie International Edition* **2017**, *56*, 987-991; bA. Rashid, G. S. Ananthnag, S. Naik, J. T. Mague, D. Panda, M. S. Balakrishna, *Dalton T* **2014**, *43*, 11339-11351.
(11) Z. Hao, X. Wu, R. Sun, C. Ma, X. Zhang, *Chemphyschem* **2012**, *13*, 267-273.
(12) D. Liu, C. He, C. Poon, W. Lin, *Journal of Materials Chemistry B* **2014**, *2*, 8249-8255.
(13) A. C. Altomare, M.; Giacovazzo, C.; Guagliardi, A., *J. Appl. Crystallogr.* **1993**, *26*, 343-350.
(14) G. M. Sheldrick, **1997**.
(15) M. J. Prakash, M. S. Lah, *Chem Commun* **2009**, 3326-3341.
(16) a) W. Liu, Y. Fang, G. Z. Wei, S. J. Teat, K. Xiong, Z. Hu, W. P. Lustig, J. Li, *Journal of the American Chemical Society* **2015**, *137*, 9400-9408; b) I. Horcas, R. Fernández, J. M. Gómez-Rodríguez, J. Colchero, J. Gómez-Herrero, A. M. Baro, *Review of Scientific Instruments* **2007**, *78*, 013705.
(17) G. Paolo, B. Stefano, B. Nicola, C. Matteo, C. Roberto, C. Carlo, C. Davide, L. C. Guido, C. Matteo, D. Ismaila, C. Andrea Dal, G. Stefano de, F. Stefano, F. Guido, G. Ralph, G. Uwe, G. Christos, K. Anton, L. Michele, M.-S. Layla, M. Nicola, M. Francesco, M. Riccardo, P. Stefano, P. Alfredo, P. Lorenzo, S. Carlo, S. Sandro, S. Gabriele, P. S. Ari, S. Alexander, U. Paolo, M. W. Renata, *Journal of Physics: Condensed Matter* **2009**, *21*, 395502.
(18) D. Vanderbilt, *Physical Review B* **1990**, *41*, 7892-7895.
(19) J. P. Perdew, K. Burke, M. Ernzerhof, *Phys Rev Lett* **1996**, *77*, 3865-3868.
(20) D. J. Chadi, M. L. Cohen, *Physical Review B* **1973**, *8*, 5747-5753.
(21) aR.-F. Song, Y.-B. Xie, J.-R. Li, X.-H. Bu, *Crystengcomm* **2005**, *7*, 249-254; bE. Cariati, D. Roberto, R. Ugo, P. C. Ford, S. Galli, A. Sironi, *Chemistry of Materials* **2002**, *14*, 5116-5123; cF. Thébault, S. A. Barnett, A. J. Blake, C. Wilson, N. R. Champness, M. Schröder, *Inorg Chem* **2006**, *45*, 6179-6187; dT. H. Kim, Y. W. Shin, J. S. Kim, S. S. Lee, J. Kim, *Inorg Chem Commun* **2007**, *10*, 717-719; eY. Takemura, T. Nakajima, T. Tanase, *Dalton T* **2009**, 10231-10243; fS.-M. Fang, Q. Zhang, M. Hu, B. Xiao, L.-M. Zhou, G.-H. Sun, L.-J. Gao, M. Du, C.-S. Liu, *Crystengcomm* **2010**, *12*, 2203-2212; gE. Cariati, D. Roberto, R. Ugo, P. C. Ford, S. Galli, A. Sironi, *Inorg Chem* **2005**, *44*, 4077-4085.
(22) G. R. Desiraju, *Angewandte Chemie International Edition in English* **1995**, *34*, 2311-2327.

(23) G. Cavallo, P. Metrangolo, R. Milani, T. Pilati, A. Priimagi, G. Resnati, G. Terraneo, *Chem Rev* **2016**, *116*, 2478-2601.
(24) aJ. K. Maclaren, J. Sanchiz, P. Gili, C. Janiak, *New J Chem* **2012**, *36*, 1596-1609; bT. Dorn, A.-C. Chamayou, C. Janiak, *New J Chem* **2006**, *30*, 156-167.
(25) J. Conesa-Egea, J. Gallardo-Martínez, S. Delgado, J. I. Martínez, J. Gonzalez-Platas, V. Fernández-Moreira, U. R. Rodríguez-Mendoza, P. Ocón, F. Zamora, P. Amo-Ochoa, *Small* **2017**, *13*, n/a-n/a.
(26) T. Okubo, N. Tanaka, K. H. Kim, H. Yone, M. Maekawa, T. Kuroda-Sowa, *Inorg Chem* **2010**, *49*, 3700-3702.

Table of Contents

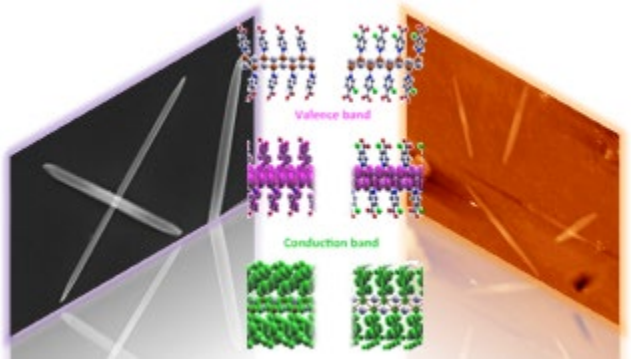

Synopsis: Structurally similar semiconducting coordination polymers based on Cu(I)-I double chains with molecular recognition has been studied. Experimental measurements and theoretical calculations show that I-Cu-I-Cu- distances and angles are the responsible of their electrical differences. Moreover, a simple bottom-up approach based on their high insolubility in the reaction medium has been used to obtain them as nanostructures.